On Solitary-Wave Solutions for the Coupled Korteweg – de Vries and Modified Korteweg – de Vries Equations and their Dynamics

Woo-Pyo Hong

Department of Electronics Engineering, Catholic University of Daegu, Hayang, Gyongsan, Gyungbuk 712-702, South Korea

Reprint requests to Prof. W.-P. H.; E-mail: wphong@cu.ac.kr

Analytic sech^4-type traveling solitary-wave solutions of the coupled Korteweg-de Vries and modified Korteweg-de Vries equations proposed by Kersten-Krasil'shchik, are found by applying the auxiliary function method. The dynamical properties of the solitary-waves are studied by numerical simulations. – PACS numbers: 03.40.Kf, 02.30.Jr, 47.20.Ky, 52.35.Mw

Key words: Coupled Korteweg – de Vries and Modified Korteweg – de Vries Equation; Analytic Solitary-Wave Solutions; Numerical Simulations; Stability; Interaction.

1. Introduction

In this paper we consider the coupled Korteweg-de Vries (KdV) and modified KdV (mKdV) equations proposed by Kersten-Krasil'shchik

$$u_t + u_{xxx} - 6uu_x + 3(vv_{xx})_{xx} - 3(uv^2)_x = 0,$$
$$v_t + v_{xxx} - 3v^2v_x - 3(uv)_x = 0,$$
(1)

which can be considered as a coupling between the KdV (with respect to u) and the mKdV (with respect to v) equations. The coupled KdV-mKdV equations were proposed by Kersten and Krasil'shchik [1] and originate from a supersymmetric extension of the classical KdV [2]. It also can be considered as a coupling between the KdV and mKdV equations: By setting $v = 0$ we obtain the KdV equation $u_t + u_{xxx} - 6uu_x = 0$; by setting $u = 0$, we obtain the mKdV equation $v_t + v_{xxx} - 3v^2v_x = 0$. In here, $(uv^2)_x$ acts as a force term on the first KdV equation, which is coupled to the second equation of similar type, without any dispersion term.

The complete integrability of the coupled KdV-mKdV equations was shown by Kersten and Krasil'-shchik by finding the existence of infinite series of symmetries and conservation laws [1]. Recently, its singular analysis and Lax pair were given by Kalkanli, Sakovich and Yurdusen, using the Painlevé test and prolongation technique [3]. More recently, a series of exact wave solutions, including the solitary wave, rational, triangular periodic, Jacobi, and Weierstrass doubly periodic solutions for (1), has been obtained by Hon and Fan [4] by using an algebraic method.

The purpose of this paper is to find new sech^4-type analytic traveling solitary-wave solutions of (1) by using the auxiliary differential equation method [5 – 8] and to investigate their dynamical behavior. In Section 2, we introduce the auxiliary differential equation method for finding the solitary-wave solutions and perform symbolic computations. In Section 3, we investigate the dynamics of the solitary-waves and their interactions by a numerical method. The conclusions are in Section 4.

2. The Auxiliary Equation Method and Analytic Solitary-Wave Solutions

In this section, we first describe the auxiliary equation method [5, 6]. Suppose given a set of coupled nonlinear partial differential equations (NLPDE) for $u(x,t)$ and $v(x,t)$ in the forms

$$H_1(u,v,u_x,v_x,u_t,v_t,u_{xx},v_{xx},u_{tt},v_{tt},u_{xt},v_{xt}\ldots) = 0,$$
$$H_2(u,v,u_x,v_x,u_t,v_t,u_{xx},v_{xx},u_{tt},v_{tt},u_{xt},v_{xt}\ldots) = 0.$$
(2)

Introducing the transformation variable $\xi = kx - \omega t$, the traveling wave solutions of $u(\xi)$ and $v(\xi)$ satisfy the following ODEs:

$$G_1(u,v,u_\xi,v_\xi,u_{\xi\xi},v_{\xi\xi},u_{\xi\xi\xi},v_{\xi\xi\xi},\ldots) = 0,$$
$$G_2(u,v,u_\xi,v_\xi,u_{\xi\xi},v_{\xi\xi},u_{\xi\xi\xi},v_{\xi\xi\xi},\ldots) = 0.$$
(3)

We seek the solution of (3) in the forms

$$u(\xi) = \sum_{i=0}^{n} u_i z^i(\xi), \quad v(\xi) = \sum_{j=0}^{m} v_j z^j(\xi), \qquad (4)$$

where u_i $(i = 1, 2, ..., n)$ and v_i $(j = 1, 2, ..., m)$ are all real constants to be determined, the orders m and n are positive integers which can be readily determined by balancing the highest order derivative term with the highest power nonlinear term in (3). The main point of the present method is to introduce $z(\xi)$ as the solutions of the following auxiliary ordinary differential equation:

$$\left(\frac{\mathrm{d}z}{\mathrm{d}\xi}\right)^2 = az^2(\xi) + bz^3(\xi) + cz^4(\xi), \qquad (5)$$

where $a, b,$ and c are real parameters. Then $z(\xi)$ is the exact solution of (5):

$$z(\xi) = \begin{cases} \dfrac{-ab\operatorname{sech}^2(\pm\frac{\sqrt{a}}{2}\xi)}{b^2 - ac\,(1 - \tanh(\pm\frac{\sqrt{a}}{2}\xi))^2} \\ \text{when } a > 0, \ \textit{type I}, \\[4pt] \dfrac{2a\operatorname{sech}(\sqrt{a}\xi)}{\sqrt{b^2 - 4ac} - b\operatorname{sech}(\sqrt{a}\xi)} \\ \text{when } \sqrt{b^2 - 4ac} > 0 \text{ and } a > 0, \ \textit{type II.} \end{cases} \qquad (6)$$

To look for the traveling wave solutions of (1) in particular, we make the transformations $u(x,t) = u(\xi)$ and $v(x,t) = v(\xi)$, leading to

$$(3v_\xi v_{\xi\xi} + u_{\xi\xi\xi} + 3vv_{\xi\xi\xi})k^3$$
$$- [6uvv_\xi + (6u + 3v^2)u_\xi]k - u_\xi\omega = 0, \qquad (7)$$
$$v_{\xi\xi\xi}k^3 + [(-3v^2 - 3u)v_\xi - 3u_\xi v]k - \omega v_\xi = 0.$$

By balancing the highest order derivative term $u_{\xi\xi\xi}$ with the highest order nonlinear term uu_ξ, we find $n = 2$. Similarly, we find $m = 1$ from the balance of vv_ξ and uu_ξ in the second equation of (1). Thus, we use the ansatz (4) for (1) as

$$u(\xi) = u_0 + u_1 z(\xi) + u_2 z(\xi)^2,$$
$$v(\xi) = v_0 + v_1 z(\xi). \qquad (8)$$

By substituting (5) and (8) into (7) and setting the coefficients of $z^j(\xi)$ $(j = 0, 1, 2, ..., 7)$ to zero, we obtain ten algebraic equations for $u_i, v_i, a, b, c, k,$ and ω. Thus,

we find two sets of solutions for the above overdetermined equations:

$$u_1 = -v_0 v_1, \ u_2 = -\frac{1}{2}v_1^2, \ \omega = -k(v_0^2 + 2u_0),$$
$$a = \frac{-v_0^2 + u_0}{k^2}, \ b = -\frac{v_0 v_1}{k^2}, \ c = -\frac{1}{4}\frac{v_1^2}{k^2}, \qquad (9)$$

$$u_0 = 2v_0^2, \ u_1 = -v_0 v_1, \ u_2 = -\frac{1}{2}v_1^2, \ \omega = -5kv_0^2,$$
$$a = \frac{v_0^2}{k^2}, \ b = -\frac{v_0 v_1}{k^2}, \ c = -\frac{1}{4}\frac{v_1^2}{k^2}. \qquad (10)$$

Equation (9) satisfies the requirement for *type I* and *type II* solutions of (6) if $a > 0$, i.e., $u_0 > v_0^2$ and if $\sqrt{b^2 - 4ac} > 0$ and $a > 0$, i.e., $\sqrt{u_0 v_1^2/k^2} > 0$ and $u_0 > v_0^2$, respectively. On the other hand, (10) also satisfies the requirement for *type I* and *type II* solutions of (6) if $a = v_0^2/k^2 > 0$ and if $\sqrt{b^2 - 4ac} = \sqrt{2v_0^2 v_1^2/k^4} > 0$, respectively. We note that $u_0, v_0, v_1,$ and k are independent parameters.

Upon substituting (9) into (8), for an example, we find two analytic solitary-wave solutions of (1):

$$u_{I,II}(x,t) = u_0 - v_0 v_1 \Lambda_{I,II}(x,t)\frac{1}{2}v_1^2 \Lambda_{I,II}(x,t)^2,$$
$$v_{I,II}(x,t) = v_0 + v_1 \Lambda_{I,II}(x,t), \qquad (11)$$

where

$$\Lambda_I(x,t) = \frac{ab\operatorname{sech}^2(\frac{\sqrt{a}}{2}(kx - \omega t))}{b^2 - ac[1 - \tanh(\frac{\sqrt{a}}{2}(kx - \omega t))]^2},$$
$$\Lambda_{II}(x,t) = \frac{2a\operatorname{sech}(\sqrt{a}(kx - \omega t))}{\sqrt{b^2 - 4ac} - b\operatorname{sech}(\sqrt{a}(kx - \omega t))}. \qquad (12)$$

In the following analysis, we only consider the set of solutions in (9) for the solitary-waves $u_{I,II}(x,t)$ and $v_{I,II}(x,t)$. As examples, we plot in Figs. 1 and 2 the profiles of the solitary-waves $u_{I,II}(x,0)$ and $v_{I,II}(x,0)$ in (11), respectively, for different sets of $u_0, v_0, v_1,$ and the wave number $k = 1$. As shown in Fig. 1, the amplitudes of $u_I(x,0)$ and $v_I(x,0)$ increase, while the widths decrease with increasing u_0 and v_0. The profiles of $u_{II}(x,0)$ and $v_{II}(x,0)$ show a similar width and amplitude dependence on $u_0, v_0,$ and v_1 as shown in Fig. 2 except that they are centered at $x = 0$. We note that both $u_{I,II}$ and $v_{I,II}$ have a nonzero background at infinity. They can be made to approach zero by taking both u_0 and v_0 close to zero, however, the width of the solitary-wave increases. The other set of
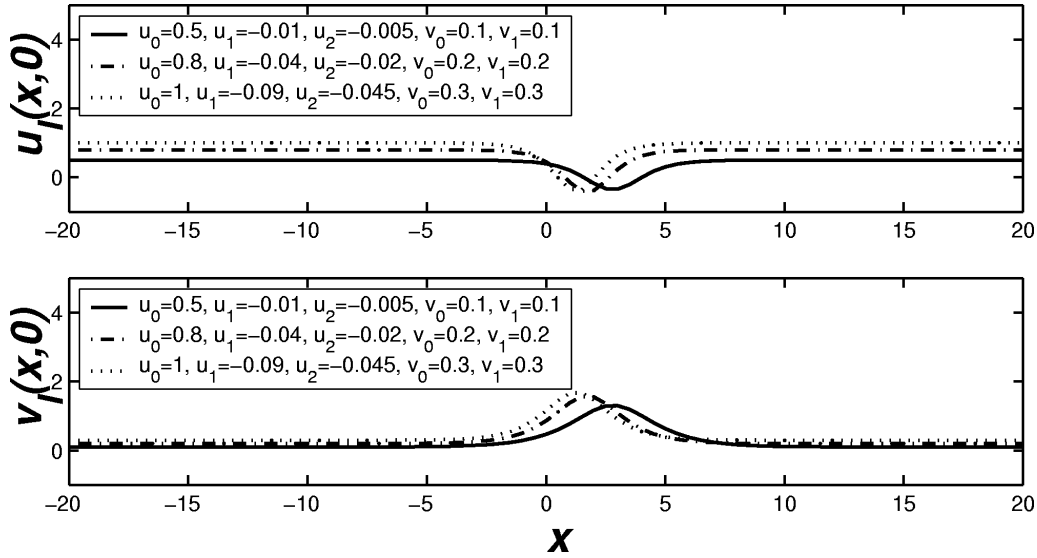
Fig. 1. The profiles of dark and bright solitary-waves $u_I(x,0)$ and $v_I(x,0)$, respectively. The amplitudes of $u_I(x,0)$ and $v_I(x,0)$ increase, while the widths decrease with increasing u_0 and v_0. The *type I* solution requires the constraint $a > 0$, i.e., $u_0 > v_0^2$ from (9).
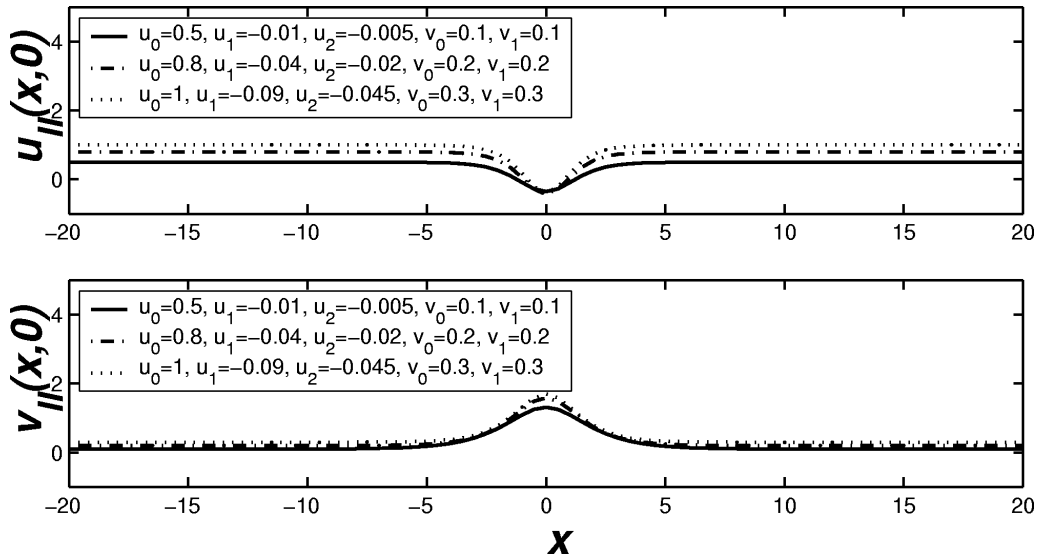

Fig. 2. The profiles of dark and bright solitary-waves $u_{II}(x,0)$ and $v_{II}(x,0)$, respectively. The amplitudes of $u_{II}(x,0)$ and $v_{II}(x,0)$ increase, while the widths decrease with increasing u_0 and v_0. The *type II* solution requires the constraint $\sqrt{b^2 - 4ac} = \sqrt{2v_0^2 v_1^2 / k^4} > 0$ from (10).

the solitary-waves corresponding to (10) shows similar characteristics as the above solutions. In the rest of this paper we investigate the dynamical properties of the solitary-waves by numerical simulations, i. e, by using the solutions in (11) as the initial wave profiles.

3. Numerical Simulations

In this section we numerically integrate (1) to understand the stability and dynamics of the solitary-wave solutions discussed in Section 2. Here the definition of "stability" means that the analytic solitary-wave pre-

$$u_0 = 0.1 \quad u_1 = -0.02 \quad u_2 = -0.02 \quad v_0 = 0.1 \quad v_1 = 0.2$$
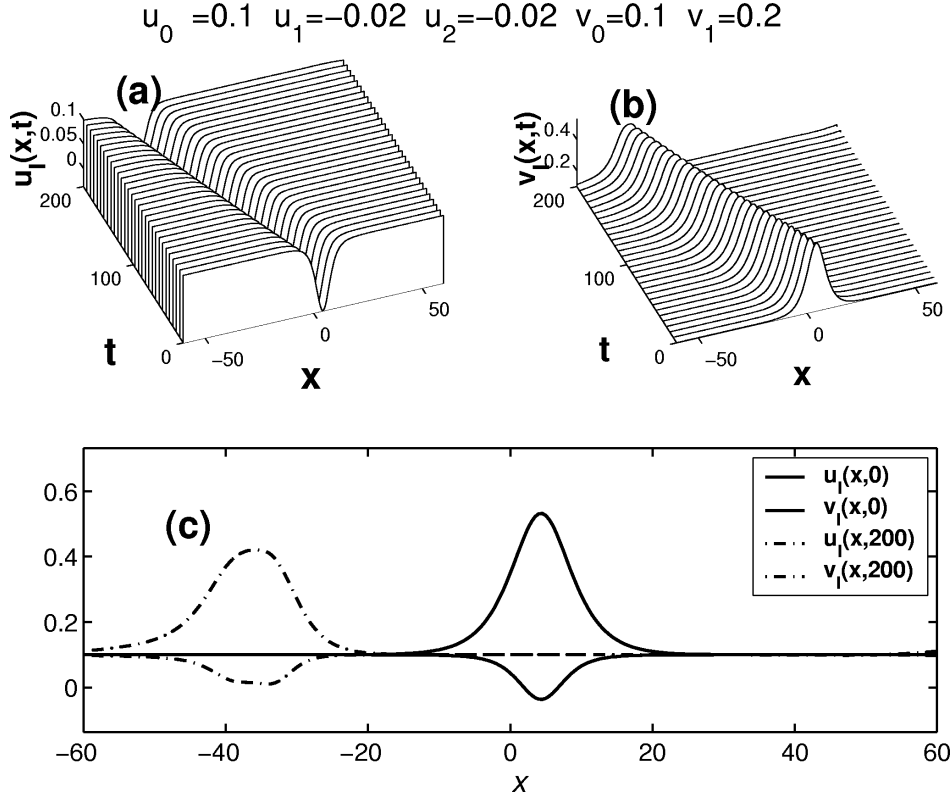

Fig. 3. (a), (b) Evolution of numerically simulated $u_I(x,t)$ and $v_I(x,t)$, respectively, with the initial profiles (13) and the wave number $k = 1$. (c) Snap shots of the dark and bright solitary-wave profiles at $t = 200$. The amplitude of both solitary-waves decreases at $t = 200$, while the width of both solitary-waves increases, compared to the initial profiles at $t = 0$. Note that the two solitary-waves have the same velocity.

serves, when it is substituted into (1) and numerically integrated, its initial profile for a long propagation time without losing its energy by radiation. The numerical scheme used in this work is based on the time advance using the Runge-Kutta fourth-order scheme and a pseudo-spectral method using the discrete fast Fourier transformation in the spatial discretization [9], applying periodic boundary conditions. The numerical errors in the spatial discretization were controlled by varying the number of discrete Fourier modes between 128 and 1024, and various time steps between 10^{-5} and 10^{-3} are chosen for a stable wave propagation.

In the following we first investigate the stability of the solitary-wave solutions by taking the initial profiles in the form

$$u_{I,II}(x,0) = u_0 - v_0 v_1 \Lambda_{I,II}(x,0) \Lambda_{I,II}(x,0)^2, \\ v_{I,II}(x,0) = v_0 + v_1 \Lambda_{I,II}(x,0). \tag{13}$$

Before proceeding, we note that (1) is in general an integrable equation since it contains an infinite series of symmetries and conservation laws as proved by Kersten and Krasil'shchik [1]. Thus we define the simplest two such integrals, namely the normalized mass and energy, as

$$M(t) = \int_{-\infty}^{\infty} \psi(x,t)\mathrm{d}x \bigg/ \int_{-\infty}^{\infty} \psi(x,0)\mathrm{d}x \tag{14}$$

and

$$E(t) = \int_{-\infty}^{\infty} \psi(x,t)^2\mathrm{d}x \bigg/ \int_{-\infty}^{\infty} \psi(x,0)^2\mathrm{d}x, \tag{15}$$

to further understand the dynamics of the waves. In (14) and (15) $\psi(x,t)$ denotes $u_{I,II}(x,t)$ and $v_{I,II}(x,t)$. However it is still questionable whether the solitary-wave solutions found in this work numerically satisfy the conservation laws.

Figures 3a and b show the evolutions of the numerically simulated dark and bright solitary-waves, $u_I(x,t)$
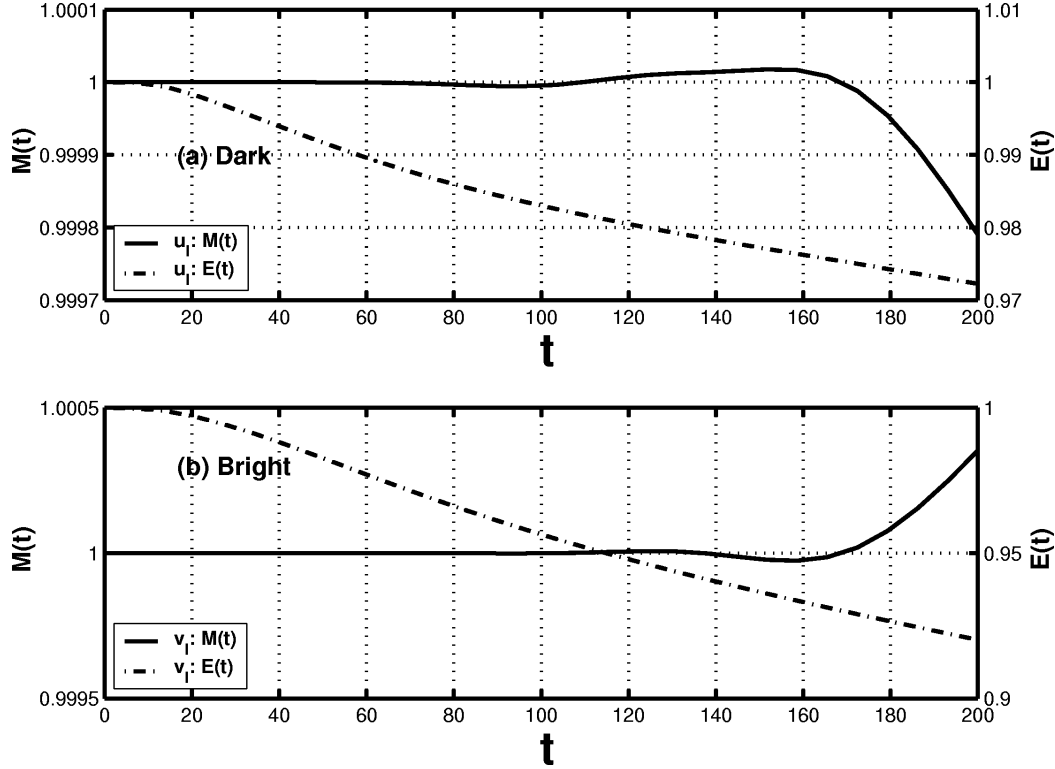
Fig. 4. (a) Evolutions of the normalized mass $M(t)$ and energy $E(t)$, respectively, for the dark solitary-wave $u_I(x,t)$ in Figure 3. The stability of the dark solitary-wave is demonstrated by the conservation of $M(t)$ (solid curve), which does hardly deviate from the initial value (less than 0.01% as shown on the left ordinate), while $E(t)$ (dot-dashed curve) deviates from its initial value (more than 2% as shown on the right ordinate). (b) $E(t)$ deviates rapidly from the initial value at $t \approx 20$, while $M(t)$ slightly deviates (less than 0.03%).

and $v_I(x,t)$, respectively, for $u_0 = 0.1, v_0 = 0.1$, and $v_1 = 0.2$, using the analytic solitary-waves as initial profiles. In the following calculations we set the wave number $k = 1$. The results demonstrate the stability of the solitary-waves up to $t = 200$ without showing radiation in the tail. However, as shown in Fig. 3c, the amplitude of both solitary-waves decreases at $t = 200$, while the width of both solitary-waves increases in comparison to the initial profiles at $t = 0$. The stability of the dark solitary-wave is more clearly demonstrated in Fig. 4a by the conservation of $M(t)$ (solid curve), which does hardly deviate from the initial value (less than 0.01% as shown on the left ordinate), while $E(t)$ (dot-dashed curve) deviates from its initial value (more than 2% as shown on the right ordinate). It is worth noting that u or v can be expressed as a conservation law from (1) as

$$(u)_t + \left[u_{xx} - 3u^2 + 3(vv_{xx})_x - 3(uv^2)\right]_x$$
$$= (u)_t + (\Gamma_1)_x = 0,$$

$$v_t + \left[v_{xx} - 3v^3 - 3(uv)\right]_x = v_t + (\Gamma_2)_x = 0, \quad (16)$$

where $\Gamma_{1,2}$ are the associated fluxes. More specifically, since the solitary-wave solutions in (11) satisfy, i.e., $u_{I,II}$, $v_{I,II} \to 0$ sufficiently rapidly as $|x| \to \infty$, it is easy to verify that $\int_{-\infty}^{+\infty} u_{I,II}(x,t)\mathrm{d}x$ and $\int_{-\infty}^{+\infty} v_{I,II}(x,t)\mathrm{d}x$ are both conserved quantities. In fact, since $\int_{-\infty}^{+\infty} \Lambda_{I,II}(x,t)\mathrm{d}x = $ const. and $\int_{-\infty}^{+\infty} \Lambda_{I,II}^2(x,t)\mathrm{d}x = $ const., $\mathrm{d}M(t)/\mathrm{d}t = 0$. Similarly, the expressions for the conservation laws of u^2 and v^2 can be obtained (see [1] for details). Even though $\mathrm{d}M(t)/\mathrm{d}t = 0$ for all t, given the numerical uncertainty, we can conclude that it is a numerically conserved quantity. On the other hand, for the bright solitary-wave case, as shown in Fig. 4b, $E(t)$ deviates rapidly from the initial value at $t \approx 20$, while $M(t)$ increases slightly from its initial value (less than 0.03%). The heuristic reason for the rapid decrease in $E(t)$ is due to the last term in (1), i.e., $-3(uv)_x$, acting as energy dissipating term. We note, that even though the evolution of the solitary-wave is
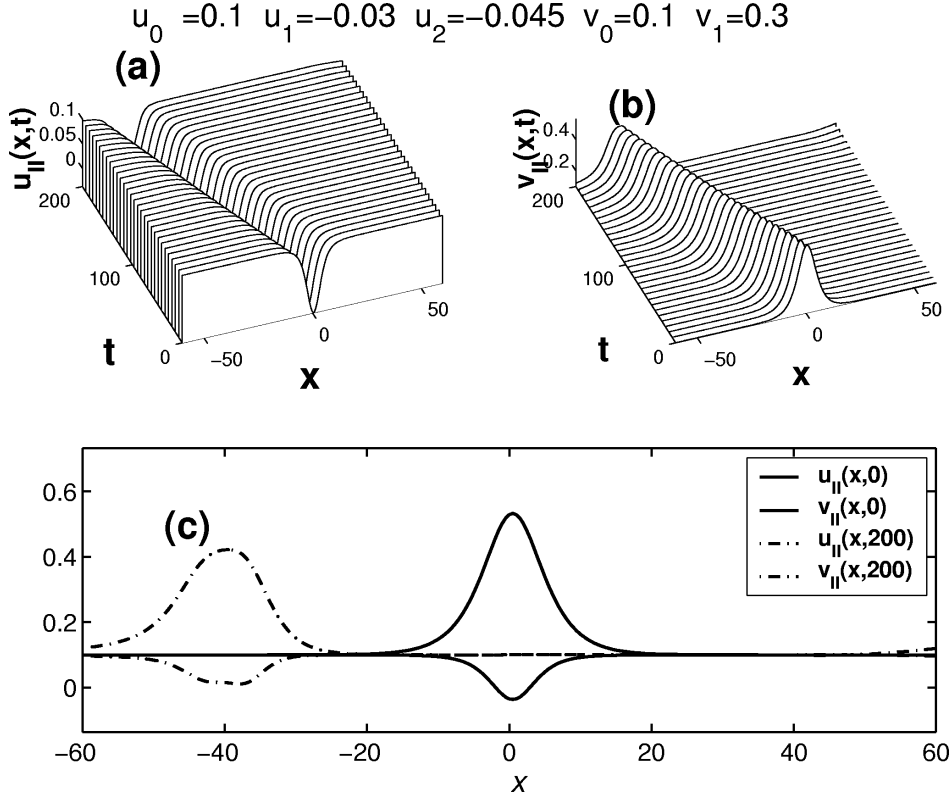
Fig. 5. (a), (b) Evolution of numerically simulated $u_{II}(x,t)$ and $v_{II}(x,t)$, respectively, with the initial profiles (13) and the wave number $k = 1$. (c) Snap shots of the dark and bright solitary-wave profiles at $t = 100$. The amplitude of the solitary-waves decreases, while the width of both solitary-waves spreads, compared to the initial profiles at $t = 0$. Note that the two solitary-waves have the same velocity.

plotted up to $t = 200$ for a clear picture drawing, the stability of the wave has been checked to maintain up to $t = 400$.

Figures 5a and b show the evolutions of the bright and dark solitary-waves of the *type II* in (13) for $u_0 = 0.1, v_0 = 0.01$, and $u_0 = 0.2$, using the analytic solitary-waves as initial profiles, which demonstrate the similar propagation characteristics as the waves in Figure 3. As shown in Fig. 5c, the amplitude of both solitary-waves decreases at $t = 200$, while the width of both solitary-waves increases, in comparison with the initial profiles at $t = 0$. The instability of dark solitary-waves is demonstrated in Fig. 6a from a large variation of $E(t)$ (more than 7% at $t = 100$) which deviates rapidly from its initial value, while the initial value of $M(t)$ is changed insignificantly (less than 0.02%). Similarly, for the bright solitary-wave case, $E(t)$ also deviates rapidly from the initial value at $t \approx 20$ and decreases continously, while $M(t)$ maintains its initial value.

Before concluding, we briefly discuss the interaction dynamics of the bright and dark solitary-waves with the initial profiles

$$
\begin{aligned}
u(x,0)_{\text{int}} &= u(x+\eta) + u(x-\eta), \\
v(x,0)_{\text{int}} &= v(x+\eta) + v(x-\eta),
\end{aligned}
\tag{17}
$$

where η is the separation between the waves. By using the same set of coefficients as in Fig. 3, as an example, the interaction dynamics of the solitary-waves separated by $\eta = 15$ is simulated and shown in Figure 7. Due to the large η, the two dark solitary-waves in Fig. 7a are initially separated, however their interaction results in a decrease of the amplitude, a decrease of the separation distance, and an appearance of oscillatory radiation on the right side, as shown in Fig. 7b at $t = 100$. Figure 7c demonstrates the variation of $M(t)$ (less than 0.01%) but an increase of $E(t)$ (about 1% increase at $t = 100$) due to the weak instability which comes from the unbalance between the dispersion and
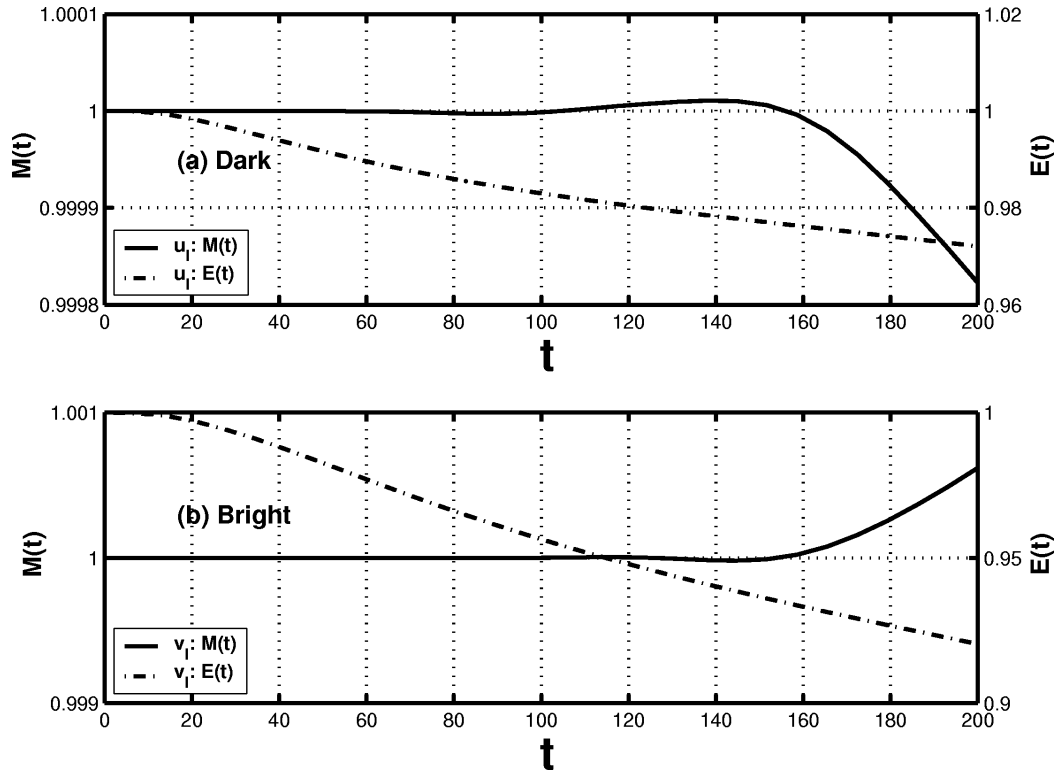
Fig. 6. (a) Evolutions of the normalized mass $M(t)$ and energy $E(t)$, respectively, for the dark solitary-wave $u_I(x,t)$ in Figure 5. The variations of $M(t)$ and $E(t)$ are very similar to those in Figure 4. (b) $E(t)$ deviates rapidly from the initial value at $t \approx 20$, while $M(t)$ slightly deviates (less than 0.1%).

nonlinear terms in (1). Figure 7d presents the evolution of two bright solitary-waves. Similar to the dark solitary-waves, the interaction results in a decrease of the amplitude, a decrease of the separation distance, but an exponentially decaying tail on the right side, as shown in Fig. 7e at $t = 100$. Even in the absence of the oscillatory radiation, this shows that the normalized energy is not conserved (about 6% decrease at $t = 100$). This instability also originates from the unbalance between the nonlinear terms in (1). After many numerical simulations with different sets of the coefficients, we find similar dynamical behaviors as presented in Figure 7. However, as η decreases down to $\eta = 5$, the two solitary-waves combine initially and begin to blow up due to the instability about $\eta = 5$.

4. Conclusions

In this work we have found four analytic solitary-waves in (11), (12) with the parameters in (9), (10) under some constraints, having nonzero background at infinity, of the coupled KdV-modified KdV equations

proposed by Kersten-Krasil'shchik [1, 2], by utilizing the auxiliary equation method [5 – 8]. We have shown in Fig. 3 by numerical simulations the dynamics of the bright and dark solitary-waves of *type I* using the analytic solitary-waves as the initial profiles and the evolutions of the normalized mass and energy in Figure 4. Depending on the sign of the coefficients of the solution, it has been demonstrated that the waves can be marginally stable in the sense that even though the amplitude and width change, $M(t)$ and $E(t)$ do not deviate from their initial values, as demonstrated in Figure 4. By taking the bright and dark solitary-waves as initial profiles, as an example, we have simulated the interaction dynamics of the waves separated by $\eta = 15$ in Fig. 7, where the interaction results in a decrease of the amplitude, a decrease of the separation distance, and a weak instability which comes from the unbalance between the nonlinear terms in (1). From these numerical investigations, we verified that $M(t)$ numerically satisfies the conservation law, while $E(t)$ seems to always deviate from the initial value, even using the highest
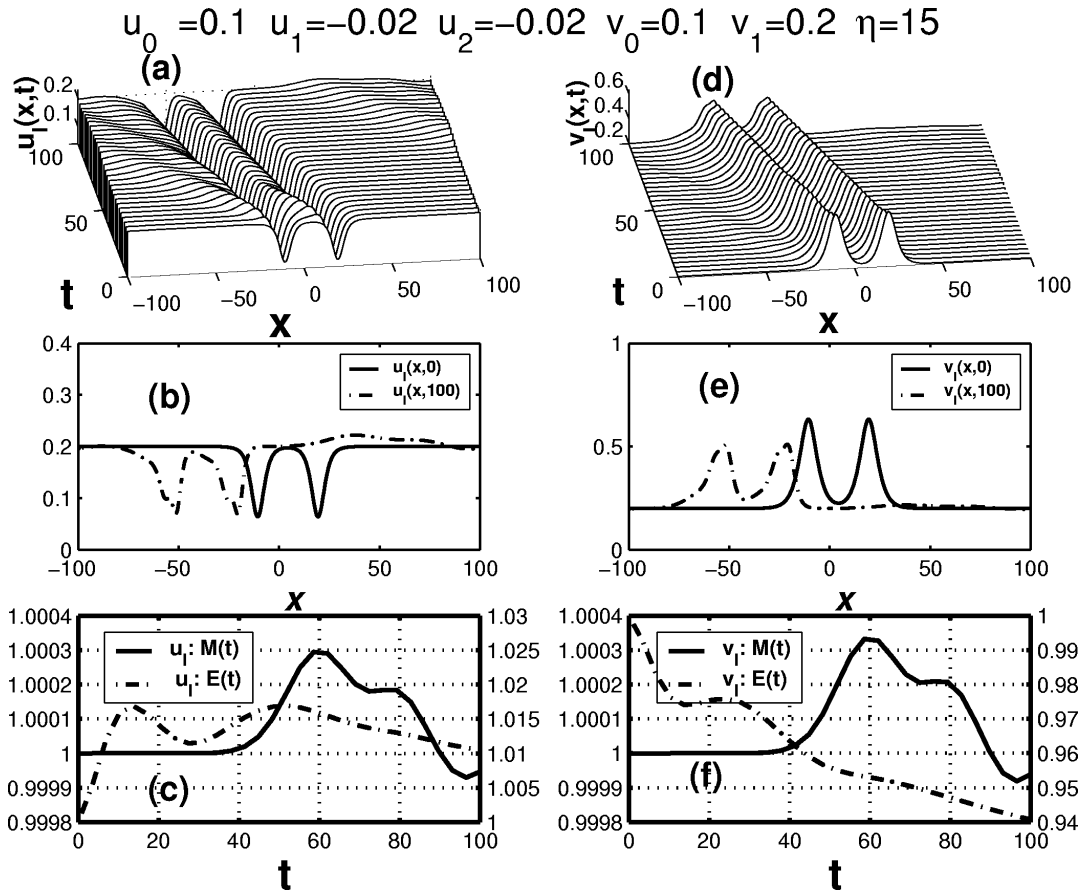
Fig. 7. Interaction dynamics of the two solitary-waves with the initial profiles in (17), where the separation is $\eta = 15$. (a), (d) Evolutions of initially separated two dark and bright solitary-waves, respectively. (b), (e) Snap shots of the numerically simulated wave profiles at $t = 100$. The separation between the two solitary-waves decreases. The oscillatory radiation on the right side in (b) and the exponentially decaying tail on the right side in (e) are shown. (c) While $M(t)$ is conserved (it deviates by less than 0.01%), $E(t)$ increases slightly from its initial value. (f) While $M(t)$ is conserved (it deviates by less than 0.02%), $E(t)$ decreases rapidly from its initial value.

numerical mesh, which indicates the violation of the conservation law. It is not certain whether the large deviation of $E(t)$ originates from the violation of the conservation law or is due to a numerical instability, which deserves a future research.

[1] P. Kersten and J. Krasil'shchik, E-print arxin: lin. SI/0010041 (2000).
[2] S. Krivonos and A. Sorin, Phys. Lett. A **251**, 109 (1999).
[3] A. K. Kalkanli, S. Y. Sakovich, and I. Yurdusen, J. Math. Phys. **44**, 1703 (2003).
[4] Y. C. Hon and E. G. Fan, Chaos, Solitons and Fractals **19**, 1141 (2004).
[5] E. V. Krishnan, J. Math. Phys. **31**, 1155 (1990).
[6] E. Yomba, Chaos, Solitons and Fractals **21**, 75 (2004).
[7] W. P. Hong and J. J. Kim, Z. Naturforsch. **60a**, 557 (2005).
[8] W. P. Hong, Z. Naturforsch. **60a**, 757 (2005).
[9] L. N. Trefethen, Spectral Method in Matlab, Siam, Philadelphia 2000.